Journal of Luminescence 252 (2022) 119408

Contents lists available at ScienceDirect

Journal of Luminescence

journal homepage: www.elsevier.com/locate/jlumin

Quantifying antisite defect concentrations in yttrium aluminum garnet by high-precision density analysis

R. Kwapisz, R.L. Cone, C.W. Thiel *

Department of Physics, Montana State University, Bozeman, MT, 59717, USA

ARTICLE INFO

Keywords:
Crystal defects
Rare-earth-doped crystals
Hydrostatic weighing
Yttrium aluminum garnet
Antisite defects

ABSTRACT

Quantifying the nature and density of lattice defects in high-quality crystals is often difficult or impossible with commonly employed material characterization techniques. In many cases, even the density of intentionally doped impurities present in a grown crystal must be inferred indirectly using methods such as mapping spatial variations in crystal properties or, when the defects are optically active, interpreting optical absorption with imprecisely known oscillator strengths. In this work we explore gravimetric techniques to obtain absolute defect densities in crystals, a powerful approach often overlooked in modern materials science. A hydrostatic weighing apparatus based on Archimedes' principle was constructed, tested, and refined to enable high-precision density measurements of small crystal samples. Application of this system is illustrated by determining the density of Yttrium Aluminum Garnet (YAG) relative to a high-purity silicon crystal density reference, minimizing traditional difficulties in correcting for the variations in surface tension and the water and air density due to small changes in ambient temperature, pressure, and solution composition. This method, using a relatively simple apparatus and small samples, is effective in measuring the intrinsic concentration of Y–Al antisite lattice defects in YAG, agreeing with results from far more elaborate high-resolution optical laser spectroscopy at cryogenic temperatures. Furthermore, we quantitatively analyze the effects of several potential sources for error, including natural variations in isotope distributions, residual surface contamination, and ambient temperature or pressure variations. Subsequently, we find that the density analysis method is a promising technique for characterizing new and modified materials being developed for applications ranging from solid-state lasers and scintillators to quantum information.

1. Introduction

In the past half century, the demand for advanced optical materials has grown significantly due to their applications in lasers, energy-efficient lighting, medical imaging, and opto-electronics. More recently, quantum computing, quantum communications, and quantum sensing have been established as key challenges in the exponentially growing technological world. In all of these applications, performance limitations include disorder and decoherence that can be caused by low levels of defects in the lattice of the optical crystals. For example, crystal defects in laser materials can lead to parasitic heating, optical damage, photodarkening, radiation sensitivity, non-radiative relaxation, and a plethora of other undesirable effects. Although they have a critical impact on many key optical technologies, the concentration and nature of these defects remains difficult to determine: many of the complex methods for characterizing crystal defects can be expensive and time consuming, often have limited sensitivity, can be difficult to calibrate, and the number and size of samples required can also limit the breadth of studies.

The presence of crystal defects is especially significant for many photonics and quantum information applications that rely on rare earth (RE) or transition metal (TM) elements incorporated into optical crystals. Large variations in quantum decoherence and spectral inhomogeneity are often observed for nominally identical crystal samples obtained from different sources, or even those grown from a single source at different times, impeding the advancement of technologies that use these materials. One example is the variation in inhomogeneous broadening and optical decoherence observed between samples for the quantum memory material Eu^{3+}:Y_2SiO_5, where evidence for glass-like two-level systems (TLS) was observed in some crystal growth runs [1]. Similarly, the optical coherence time of Tm^{3+}:YGG was found to be limited by TLS even in the highest quality crystals, requiring lower

* Corresponding author. Physics Department, EPS 264, Montana State University, Bozeman, MT, 59717, USA.
E-mail address: thiel@physics.montana.edu (C.W. Thiel).

https://doi.org/10.1016/j.jlumin.2022.119408
Received 5 July 2022; Received in revised form 22 September 2022; Accepted 8 October 2022
Available online 12 October 2022

temperatures to reach the performance needed for quantum repeater applications [2,3]. Defects and variations in material stoichiometry have also been found to limit the coherence lifetimes of Er^{3+}:$LiNbO_3$ powders and to dramatically affect inhomogeneous broadening and nuclear hyperfine lifetimes for Tm^{3+}:YAG [4,5].

High-precision density measurements are an often overlooked but potentially powerful method for studying stoichiometry and defect concentrations in solid-state materials science. At the simplest level, direct measurement of changes in mass can often be used to evaluate modification to the composition of individual samples caused by ion indiffusion or outdiffusion. A prominent example is the work by Johnson et al. [6] to determine the density of indiffused H^+ and D^+ in TiO_2 and thereby provide one of the very few absolute calibrations of the transition oscillator strength for the O–H and O-D fundamental vibrational mode infrared transitions in crystals—a result that has been widely used over the decades since that work was reported. Nevertheless, more elaborate measurements of density rather than mass are generally required to evaluate changes in composition between different samples or materials. Density measurements may be performed with very high precision by using hydrostatic weighing methods, and an extensive body of literature exists on the techniques and refinements that enable exceptional precision and accuracy to be achieved (for examples, see the review by Fujii [7] and the work cited therein).

1.1. Rare-earth-doped yttrium aluminum garnet crystals

In this work, we apply the hydrostatic weighing method to address the longstanding question of the absolute density of Y–Al antisite defects in the optical material yttrium aluminum garnet (YAG). YAG was chosen to demonstrate the power of the density measurement method due to its relevance in modern photonics and quantum systems coupled with the extensive range of past high-resolution optical studies that have been carried out on the intrinsic lattice defects [8,9]. YAG is a well-known host material for RE ions, which have electron configurations that are optimal for obtaining sharp optical transitions with high quantum efficiency [10,11]. YAG is also used in spectral hole burning applications such as optical signal processing and laser frequency stabilization for quantum information science [10]. The dominant point defect in many rare-earth (RE) doped garnets is thought to be antisite occupation of Y^{3+} or the rare earth dopant on the Al^{3+} site in the host crystal structure [8,9,12,13]. These antisite defects are believed to be the cause of the large inhomogeneous broadening observed for the optical transitions of RE-doped crystals used in photonic and quantum technologies [8–10,14]. Our goal was to test a quick, easy, and inexpensive method for measuring the absolute concentration of naturally occurring crystal antisite defects in Czochralski grown yttrium aluminum garnet (YAG). Furthermore, this study provides an example of how crystal density analysis may be used to quantitatively study defects and material quality more broadly for cases where it is applicable, such as oxygen vacancies, interstitial hydrogen impurities, and rare-earth or transition metal doping concentrations.

Rare-earth-doped garnets are key optical materials that are employed in the widest range of traditional luminescence applications of any RE-doped crystal, including white light LEDs [15,16], solid-state lasers [17–19], ceramic lasers [19,20], single-crystal optical fibers [21], cathode ray tubes, fluorescent lamps, dosimeters, afterglow materials, and scintillators [16,22]. Garnets are a complex oxide crystal with a 160-atom body-centered-cubic unit cell composed of eight formula units of $A_3B_2C_3O_{12}$. A, B, and C are trivalent cations and O represents the divalent oxygen anion O^{2-}. Three sites make up the garnet structure: cations A, B, and C are located in the Wyckoff c-, a-, and d-sites with dodecahedral, octahedral, and tetrahedral coordination of oxygen anions (with D_2, C_{3i}, and S_4 symmetries, respectively) [9,23].

1.2. Antisite defects in YAG

In perfect YAG ($Y_3Al_5O_{12}$), twenty-four Y^{3+} ions occupy the larger dodecahedral c-sites, sixteen Al^{3+} occupy octahedral a-sites, and twenty-four Al^{3+} occupy tetrahedral d-sites. However, during the growth stages of real garnets, the formation of crystal defects is almost unavoidable. Theoretical calculations performed on the atomic structure of YAG have consistently found that, of all potential defects in the garnet structure, antisite defects where Y^{3+} replaces Al^{3+} at an a-site in the lattice requires the least energy to form and are therefore expected to have the greatest concentration of any intrinsic defect [24–32]. In contrast, antisites involving Y^{3+} replacing Al^{3+} at lattice d-sites and Al^{3+} replacing Y^{3+} at the c-site require greater energy to form and will thus have significantly lower concentrations in the as-grown crystals.

Spectroscopic characterization of YAG attributes several spectral lines from UV to near-IR to crystal impurities. Specifically, two lines at 260 and 320 nm are thought to be caused by Y–Al antisites and other correlated defects, such as Fe^{3+} impurities and oxygen vacancies [12,23,33–37]. It is widely recognized that crystals with higher defect concentrations have poorer optical quality [33,38]. Research has also shown that YAG grown at temperatures below 1200 K has very low concentrations of antisites [31,39], in contrast to the crystals grown directly from stoichiometric melt at higher temperatures. Correlations have also been drawn between crystal growth method and defect concentrations [35].

Despite the large number of studies, there are many discrepancies in the estimated concentration of intrinsic defects in YAG. Previous work on ion substitutions in double oxides as a function of ionic radius has given models for RE^{3+} defect concentrations in rare-earth-doped garnets [40,41]. However, none of the sources obtain quantitative concentrations of antisite defects in YAG with those approaches. Studies that go beyond relative spectral line intensities generally report concentrations to be somewhere between 0.1 and 15 atomic percent [8,23,42–44]. This corresponds to a value of x ranging from 0.001 to 0.15 in the molecular formula $Y_3(Al_{1-x}Y_x)_2Al_3O_{12}$. Incongruity in these measurements is likely due to the limited accuracy of the methods combined with the dependence of antisite defect formation on growth temperature [28]. At the typical growth temperature of 2273 K, the percent concentration of Y–Al antisites is estimated to reach 0.23%; however, at 2000 K, this number can drop to 0.1% [31]. Crystals grown from melt-solution (flux growth) require much cooler temperatures than their bulk grown counterparts. The intensity of the 260 nm transition in single-crystalline films (a representative of the flux grown garnet) is significantly smaller than that of bulk crystals, leading to the conclusion that thin-film samples can contain much smaller percentages of Y–Al antisite defects [23]. Quantitatively characterizing these types of differences between crystals grown by different methods or sources was a central motivation for developing a cheap, simple, and relatively quick method for determining defect concentrations.

Perhaps the most relevant results to our characterization of YAG antisites are measurements done on Er^{3+} substitutions for the C_{3i} symmetry Al^{3+} sites. Spectroscopic techniques were used to determine an Er^{3+} occupation of 0.6 atomic percent in C_{3i} symmetry sites [9]. The ionic radius of erbium (0.890 Å) is a slightly better match of the aluminum's small radius (0.535 Å) than that of the Y^{3+} in octahedral sites (0.900 Å) [45], which may affect the formation of antisite defects. In this work we verify those optical results using a completely independent technique, finding good agreement and also further improving the accuracy of the estimated antisite density concentration.

2. Method

Typically, defect densities are determined by methods including x-ray diffraction, photoluminescence, Rutherford backscattering, mass spectroscopy, x-ray fluorescence, cathodoluminescence, positron annihilation spectroscopy, extended x-ray absorption fine structure, Raman

imaging, thermoluminescence, and other types of spectroscopy [12,39,44,46,47]. While these methods can yield high-precision results in some cases, they are often only applicable to specific types of defects or materials and typically suffer from matrix effects that make absolute calibration of results difficult. In contrast, density methods can be applied to any material and provide absolute measurement results but can be limited by the need to interpret the observed density variations as a specific type of dominant defect in the material. Even so, density measurements are particularly powerful when studying systematic changes in materials, such as the results of material processing or variation in doping concentrations, providing an unambiguous approach for assigning changes in density.

Density measurements using the hydrostatic approach have been successfully applied previously in studies of crystal stoichiometry and defect concentrations. A prominent example is the evaluation of Li^+ and Nb^{5+} vacancy models, antisite densities, and crystal stoichiometry in $LiNbO_3$ [48–51]. As another type of application, density measurements have also been used to evaluate the change in molar volume of phosphate glasses as the composition is varied [52]. An example of a third type of application is the use of density measurements to quantitatively determine the concentration of H^+ and D^+ impurities diffused into TiO_2 crystals [6]. Yet, very little research has been done within the past few decades using the density method to characterize crystal defects.

2.1. The hydrostatic method for determining density

Many methods have been employed in the past for precision density measurements. These approaches can largely be divided into two classes of techniques: volumetric, or displacement, methods and hydrostatic methods. The volumetric methods rely on precisely determining the volume and mass of on object independently and then calculating the density from those measurements. This can be carried out by precise measurement of sample dimensions, sometimes employing interferometry [53], or by using a volumetric measuring apparatus such as a gas pycnometer and Boyle's Law to determine volume [54]. While these methods can approach absolute fractional accuracies of 10^{-8} under some conditions, the second group of measurement technique using hydrostatic weighing can be applied more generally for solids with greater precision, especially for smaller or irregularly shaped samples [55]. The hydrostatic weighing approach is based on Archimedes' principle where a change in apparent weight of a sample due to buoyancy forces when submerged in a liquid can be directly used to determine the sample density relative to the known liquid density [54]. The hydrostatic method can readily achieve relative precision in the few parts-per-million range with a simple apparatus if corrections for systematic errors such as surface tension, temperature, and pressure variations are taken into account [56,57], and precision down to the 10^{-7} range or better is possible with more sophisticated experimental designs [58–60]. Consequently, hydrostatic weighing has been used to measure the density of high-purity silicon National reference standards [56,58,61] as well as in absolute determinations of Avogadro's constant [60]. For extensive reviews of the hydrostatic weighing method and its refinements, see Refs. [7,54,55,57,62].

The hydrostatic weighing method involves measuring the change in apparent weight when a sample is submersed in a fluid versus when weighed in air. When placed in a fluid, the solid will experience a force equal to the weight of the fluid that it displaces (Archimedes' Principle). If the density of the fluid is known, the change in apparent weight can be used to determine the density of the solid using the simple relation

$$\rho_s = \rho_f \left(\frac{m_s}{m_s - m_{sf}} \right) \tag{1}$$

where ρ_s is the density of the sample, ρ_f is the density of the fluid, m_s is the weight (or mass) of the sample, and m_{sf} is the weight (or apparent mass) of the sample when submersed in the fluid.

2.2. Absolute determination of crystal density

Very high accuracy and precision must be achieved in density measurements to enable calculations of defect concentrations when they exist at low densities in a crystal sample. Traditional hydrostatic weighing work has usually relied on knowing the exact density of the working fluid, which can be problematic due to several factors, including the dependence of fluid density on ambient temperature and pressure, adsorption of gases into the fluid, impurities that may be present such as the surfactants that are often needed, buoyancy of the weighing pan and wire that supports the test sample, among others. In addition, the surface tension of the fluid leads to meniscus effects and corresponding forces on the suspension wire that depend critically on the conditions and that are hard to predict.

All of these sources of error can be eliminated by using a reference sample of known density to *measure* the density of the solution at the time of weighing a test sample. With this approach, the same corrections due to variations in buoyancy and surface tension forces affect both the reference and sample measurements so that the effects are eliminated from the density calculation. With the use of a known density reference, the calibrated sample density can be directly calculated from the relation

$$\rho_s = \rho_r \frac{m_{sa}\left(m_{ra} - m_{rf}\right)}{m_{ra}\left(m_{sa} - m_{sf}\right)}. \tag{2}$$

where ρ_s (ρ_r) is the sample (reference) density, m_{sa} (m_{ra}) is the sample (reference) weight in air, and m_{sf} (m_{rf}) is the apparent sample (reference) weight when submersed in the fluid.

For this work, high-purity single-crystal silicon was chosen for the reference standard due to its very precisely known density of 2.329074 $\pm$ 1.6 $\times$ 10^{-6} g/cm^3 [61]. The particular reference sample used for all measurements was a 1-cm silicon cube cut from a 99.999% purity crystal boule. All faces were polished to optical quality and the edges were rounded to avoid chipping. The high purity of the reference sample makes any uncertainty in the reference density negligible compared to other sources of error.

For the YAG test crystal sample, a crystal grown by the Czochralski method using starting materials with 99.999% (5 N) purity was used. Published results on YAG suggest that 5 N Czochralski grown crystals have less than 10 ppm of total impurities [34]. Using these results, a rough estimate of the density uncertainty can be made. By averaging the impurity mass over all estimated impurity ion densities, the maximum uncertainty on antisite concentration due to purity would be less than 0.01%.

Ten independent variables are used to calculate the antisite defect concentration. Six variables are constants pertaining to the test crystal properties and four are the balance measurements of the reference and sample crystals. The antisite defect concentration c was found from the equation

$$c = \frac{M_F}{N_H(M_D - M_H)} \left(\frac{\rho_s}{\rho_0} - 1 \right), \tag{3}$$

where ρ_s is the measured sample density, ρ_0 is the ideal density calculated from the stoichiometric composition and lattice parameter, M_F is the formula mass of a unit cell of the crystal (8 $\times$ $Y_3Al_5O_{12}$), M_H is the mass of the natural site occupant (Al), M_D is the mass of the antisite defect (Y), and N_H is the number of potential defect substitution sites in a unit cell (8 $\times$ 2).

The formula mass M_F of stoichiometric YAG is calculated using the average host ion atomic masses for natural isotopic abundance taken from the 2015 IUPAC technical report (88.90584 g for Y, 26.98154 g for Al, and 15.99940 g for O) [63]. The ideal density is then found using a unit cell parameter of 12.0085 $\pm$ 0.0001 Å that previously has been measured for Czochralski-grown YAG [64]. Together, this gives an ideal

crystal density for stoichiometric YAG of 4.5539 ± 0.0011 g/cm^3.

3. Experimental details

Fig. 1 displays the weighing apparatus and its components used for the hydrostatic density measurements. The weighing frame was 3D printed using fused deposition modeling as a single piece to be as light as possible. Polylactic acid (PLA), acrylonitrile butadiene styrene (ABS), and high-impact polystyrene (HIPS) were each investigated and tested as construction materials, with the final system made from PLA. While PLA has a slightly higher density of 1.24 g/cm^3 (as opposed to 1.04 and 1.03 g/cm^3 for ABS and HIPS), providing a larger baseline mass that must be subtracted from the measurements, it has much greater "stiffness" as quantified by a flexural modulus of 3.8 GPa (the flexural modulus for ABS and HIPS is about 2 and 2.3 GPa, respectively) [65]. It was found that the greater stiffness more than compensates for the higher density, allowing smaller part cross-sections and overall lower weight with greater stability. The frame was annealed above the PLA glass transition temperature (~65 °C) at a temperature of 80 °C for several hours to relax strain and increase crystallization of the plastic, which significantly increased both the tensile and flexural strength of the frame [66].

The apparatus consisted of a base plate with an arch and two weighing pans. On top of the arch was the upper pan for measuring the dry weight of a crystal sample. An arm extended down to the second pan, which was used for measuring the submerged crystal weight. To reduce surface tension and buoyancy effects on the frame, a thin piece of steel wire was inserted into the arm where it entered the solution. A beaker that was filled with the water and surfactant solution was supported on a stand above the balance weighing pan so that only the plastic frame was in contact with the balance pan.

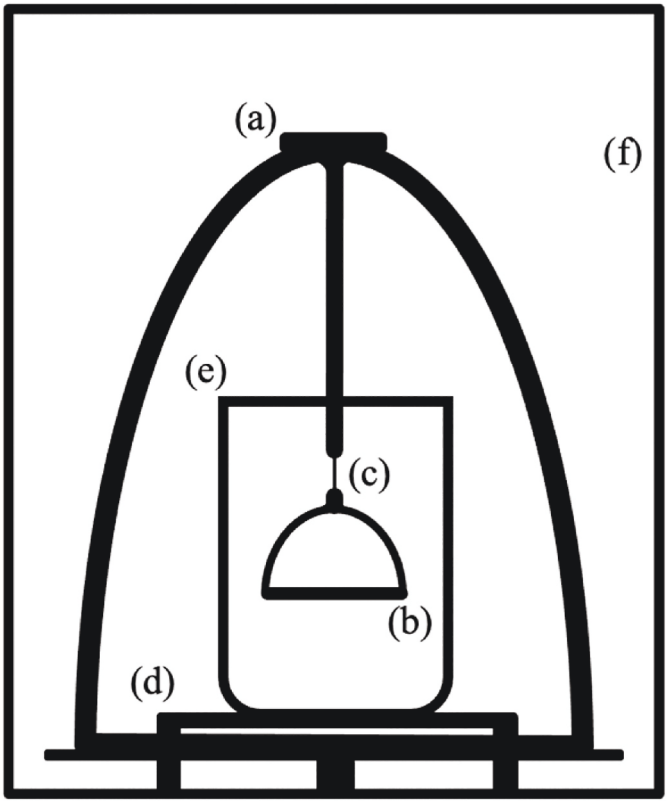

Fig. 1. The hydrostatic weighing apparatus: (a) Upper weighing pan for weight in air; (b) Submerged weighing pan for weight in working fluid; (c) Steel suspension wire; (d) Beaker stand to support the beaker above the balance pan; (e) Beaker holding working fluid; (f) Balance chamber that prevents air currents from disturbing measurements.

A common challenge with the hydrostatic weighing method is the formation of air bubbles on the surface of both the submerged weighing pan and test crystal. Air bubbles can change the scale reading by up to a milligram, which corresponds to roughly a 0.2% difference in the calculated defect concentration. To minimize the effects of bubbles and meniscus effects around the suspension wire, deionized water was mixed with 100:1 parts Triton X-100, 10:1 parts polyethylene glycol 400, and 10:1 parts Liquinox to simultaneously address different types of potential surface contaminants and used as the working fluid. The addition of the mixture of surfactants to the water solution greatly reduced the formation of air bubbles. The density of the solution varied slightly between measurements due to small changes in composition as well as variations in ambient temperature and pressure, with measured fluid densities ranging between 1.0017 g/cm^3 and 1.0049 g/cm^3.

The analytical balance used for the weight measurements was a RADWAG AS 82/220.R2. In the 0.001–82 g range used for this work, the balance has a specified repeatability of 1.5×10^{-5} g at 5% maximum capacity. For the roughly 3.8 g Si reference mass used, the experimentally observed error was 2.1×10^{-5} g, which is comparable to the balance specification.

To ensure crystals were free of any particulates, oils, or other surface contaminants before measurement, they were placed in a surfactant solution and sonicated for 60 s. They were then rinsed with ethanol to remove any of the surfactant residue. Care was taken to keep the sample and reference from being contaminated during the measurement process.

As the first step in the weighing process, the silicon control crystal was weighed in air. Before measuring the submerged weight, it was submerged in a beaker with an identical mixture of surfactants as the suspension fluid. This step coated the outside of the crystal with liquid to prevent air bubbles from forming when it was placed in the suspension fluid beaker. The test crystal was then weighed in the same manner. The two crystals were weighed eight times each for each measurement run. It was important to ensure the crystals were cleaned with ethanol between each weighing; for a centimeter cube sized crystal, the residue of the surfactant solution weighed 3.4×10^{-5} g, which is a large enough change in mass to have a significant effect on the measurement if the residue is not carefully removed.

4. Results

The crystal studied in this work was a 4.5295 g rectangular sample of YAG that was optically polished flat on all sides and with care to avoid chipping on the edges. The crystal was grown by the Czochralski method using starting materials with 99.999% (5 N) purity (crystal sample #12–667) by Scientific Materials Corporation (a division of Teledyne-FLIR). The crystal was annealed in air to minimize any residual oxygen vacancies and the YAG sample studied did not exhibit any observable coloration, further indicating a very low oxygen vacancy concentration [67]. The measured density of the sample was 4.5579 ± 0.0005 g/cm^3, whereas the ideal density of a stoichiometric YAG sample is 4.5539 ± 0.0011 g/cm^3.

The increased density of the crystal relative to the ideal density corresponds to a calculated antisite density of 0.42 ± 0.13 at. % of Y^{3+} ions occupying the C_{3i} symmetry Al^{3+} sites or, equivalently, x = 0.0042 for $Y_3(Al_{1-x}Y_x)_2Al_3O_{12}$. Standard errors in dry and submerged weighing of the sample averaged to 1.3×10^{-4} and 3.9×10^{-4} respectively.

Our procedure is further validated by a high level of repeatability in measurement. Results from two trials of eight weighings of the sample at different times had a mean of 0.42 at. % and standard deviation of 0.07 at. %. The sixteen measurements taken all fall within the 95% confidence interval of ± 0.13 at. %.

Many factors were considered when calculating the error bars on the estimate of the antisite density, several of which had too small an effect to be included in the final calculation. The total error is modeled based

on the individual uncertainties in the values of the ten input variables, which were assumed to be independent and Gaussian. With the assumption of independent random variables, the total variance is calculated by summing the individual contributions determined by the partial derivatives with respect to each variable and the estimated uncertainty in that variable. Consequently, the total uncertainty Δc in the estimated atomic percent antisite defect concentration is given by

$$\Delta c = \sqrt{\sum_i \left(\frac{\partial c}{\partial x_i}(\Delta x_i)\right)^2} \tag{4}$$

Where the x_i variables are general labels representing the ten parameters enumerated in Table I. The values of all parameters that contribute to the antisite defect model and their fractional uncertainties are given in Table I In addition, the fractional contributions to the total variance of the estimate are given in the table, revealing that the value of the ideal crystal density is the largest source of uncertainty in our estimate, with the weight of the sample when submersed in the fluid the second largest contribution to the total error. This analysis shows that our measurement procedure is sufficient to estimate the antisite defect density to a precision better than what is possible due to the uncertainty in the known lattice parameter of YAG.

5. Discussion

The measured antisite defect concentration of 0.42 ± 0.13 at. % found with our approach is slightly lower than the value estimated in previous research. Our result definitively rules out some of the very high estimates for the defect concentration that are greater than 1% [44], and more closely agrees with estimates suggesting concentrations between 0.1 and 1% [9,31]. In particular, the previous study using optical spectroscopy on erbium-doped YAG found that the density of Er^{3+} ions occupying the C_{3i} Al^{3+} site was near 0.6 at. % [9]. The approach used in that work was to identify the absorption lines in the spectrum due to Er^{3+} at sites with the C_{3i} symmetry and then use optical nutation measurements to calculate the transition dipole moment from the Rabi oscillations and use that result with the integrated absorption coefficient to calculate the number density of Er^{3+} ions at the C_{3i} sites. While the uncertainty in the previous result is unknown, given that the atomic radius of Y^{3+} in octahedral sites is slightly larger than that of Er^{3+} [45], it is possible that Y^{3+} could have a lower occupation of the much smaller Al^{3+} lattice sites than Er^{3+}. Thus, the small difference between our result and the previous measurement using Er^{3+} as a probe ion could be due to a dependence of antisite formation probability on the cation ionic radius. Research into the effect of different growth methods on the concentration of antisites is limited; although it is widely presumed that flux grown YAG contains a lower quantity of defects than crystals grown by the Czochralski method since lower temperatures are required, for example. It is possible that the samples of YAG used for our measurements had a lower concentration of antisites than those used in previous research; this possibility could be explored by carrying out a series of density measurements on Czochralski-grown YAG samples from different sources.

In the following sections, we quantitatively analyze potential sources of error in the hydrostatic weighing approach and show that none of them significantly affect our estimate for the antisite defect density.

5.1. Effect of ambient temperature and pressure variations on measurement uncertainty

The first potential source of error that we consider is the effect of temperature changes on the balance as well as the densities of the sample, the reference, the working fluid, and the surrounding atmosphere. The balance used in this work has a specified temperature sensitivity of $1 \times 10^{-6}/°C$. To determine if thermal drift could contribute errors to the measurements, the ambient temperature of the room was monitored and found to vary by much less than 0.1 °C over the ~10 min timescale of a measurement run, and hence this is expected to be a negligible source of error as compared to our observed experimental fractional uncertainty of 2.4×10^{-4}.

The thermal expansion coefficient of YAG at 24 °C is $6.8 \times 10^{-6}/°C$ [68], and the thermal expansion Δl is related to the change in crystal volume ΔV, and hence density $\Delta\rho$, according to

$$\left|\frac{\Delta\rho}{\rho}\right| = \frac{\Delta V}{V} = 3\frac{\Delta l}{l} \tag{5a}$$

As a result, the uncertainty in the density of YAG due to temperature variations is $2.0 \times 10^{-5}/°C$, which is significantly below the uncertainty in our measurements. We should note that since we do not know the exact temperature at which the lattice constant was measured [64], there is an estimated contribution of $\sim 1 \times 10^{-5}$ to the absolute uncertainty in the ideal density of the crystal due to thermal expansion, which is still less than our experimental uncertainty. For the silicon reference crystal, the thermal expansion is $2.6 \times 10^{-6}/°C$ at 24 °C [69], corresponding to an uncertainty of $7.8 \times 10^{-5}/°C$, which contributes a negligible uncertainty to our measurement.

Also, we should note that there is an uncertainty in the density of the samples due to the variation in air pressure; however the bulk modulus is 180 GPa for YAG [70] and 98 GPa for silicon [71], contributing negligible fractional uncertainties that are in the range of 10^{-8} for any practical conditions.

For the water solution used in the hydrostatic weighing, the temperature dependence of the density is $2.5 \times 10^{-4}/°C$ at 24 °C [72], which is well below our experimental uncertainty for the <0.1 °C temperature variations. When weighing the dry samples, we must also consider the contribution of buoyancy due to the air. For our experimental conditions of 24 °C and an ambient air pressure of 86 kPa, the density of air is 1.01×10^{-3} g/cm^3 [57], contributing an absolute fractional change of 2×10^{-4} to the observed density of the sample. However, by using the silicon crystal as a density calibration reference, this contribution to the density measurements is eliminated in a similar fashion as for the working solution density. As a result, the measurement is only affected by the much smaller change in density with temperature and pressure, contributing a negligible uncertainty of less than 1×10^{-6}

Table 1
Input parameters and their uncertainties (see text). The rightmost column is the percent contribution of the individual parameter uncertainties to the total variance. (* per unit cell).

Parameter	Label	Value	Fractional Uncertainty	Contribution to Total Variance
crystal stoichiometric formula mass*	M_F	593.61 g/mol	0.01	< 0.1%
defect mass	M_D	88.90584 g/mol	2×10^{-7}	< 0.1%
host atom mass	M_H	26.98154 g/mol	1×10^{-7}	< 0.1%
number of host substitution sites*	N_H	16	0	0
ideal stoichiometric test crystal density	ρ_0	4.5539 g/cm^3	1.1×10^{-3}	67.8%
reference mass when measured in air	m_{ra}	3.81069 g	2.1×10^{-5}	< 0.1%
apparent reference mass when submerged in fluid	m_{rf}	2.1668 g	1.2×10^{-4}	7.6%
reference density	ρ_r	2.329074 g/cm^3	1.6×10^{-6}	< 0.1%
sample mass when measured in air	m_{sa}	4.52963 g	4.2×10^{-5}	1.5%
apparent sample mass when submerged in fluid	m_{sf}	3.5310 g	1.3×10^{-4}	23.0%

to our measurements.

5.2. Contributions from residual surface contamination

Among the factors considered in our analysis is the uncertainty in measured density due to potential contamination on the surface of the sample. For a cubic sample with a uniform, thin layer of contamination, the uncertainty in the density is described by

$$\frac{\Delta\rho}{\rho_0} \approx \frac{6 \bullet t}{l}\left(1 - \frac{\rho_c}{\rho_0}\right) \tag{5b}$$

where t is the thickness of the contamination layer, l is the side length of the cube, ρ_c is the density of the contaminant, and ρ_0 is the true density of the sample. Contamination of the ultrasonic cleaned YAG samples was measured to be less than 1 nm thick using both x-ray photoelectron spectroscopy (XPS) and secondary ion mass spectroscopy (SIMS) depth profiling, indicating that residual surface contamination is a negligible factor for our samples. For example, if we assume that a 1 nm residual layer of the suspension fluid remains on the sample when weighing in air, causing a contamination with a density of $\rho_c \approx 1$ g/cm^3 on the surface of the crystal with $l = 1$ cm and $\rho_0 = 4.5$ g/cm^3 (typical values for our samples), the uncertainty in measured density is approximately 4.6 $\times 10^{-7}$ g/cm^3. While this is too little to change the measured density in our studies, this highlights the need to carefully clean the samples since a layer of a few hundred nanometer thickness would be enough to begin to affect the measurement accuracy.

5.3. Uncertainty due to natural isotope distribution variations

Random variations in isotope composition are common in naturally occurring minerals obtained from different parts of the world, and therefore also the growth starting materials that are synthesized from them, potentially providing a source of uncertainty in the measurements that has been overlooked in past work using density to probe defect concentrations. For the case of YAG studied here, oxygen is the only element with more than one stable isotope. The minority oxygen isotopes are ^{18}O with 0.205% natural abundance and ^{17}O with 0.038% natural abundance, and the fractional variation in the isotope ratios relative to the majority ^{16}O isotope are commonly denoted as δ^{18}O and δ^{17}O [73]. Since the abundance of ^{17}O is much lower than ^{18}O, we ignore its contribution to the uncertainty in the density. The actual isotope ratio $R_{18/16}$ is related to the delta parameters and a nominal average ratio R_0 of 0.00205 according to the following definition.

$$R_{18/16} = \left(\frac{\delta^{18}O}{1000} + 1\right)R_0 \tag{6}$$

In the limit that of $R_{18/16} \ll 1$, we can simply derive the fractional uncertainty in density due to an uncertainty in the isotope ratio as

$$\frac{\Delta\rho}{\rho_0} \approx \frac{N_O(M_{18} - M_{16})}{M_F}\Delta R_{18/16} = \frac{N_O(M_{18} - M_{16})}{M_F}\left(\frac{\Delta\delta^{18}O}{1000} + 1\right)R_0 \tag{7}$$

where N_O is the number of oxygen per formula unit, M_{18} and M_{16} are the isotope masses. The maximum range of δ^{18}O values observed is roughly 30 for natural minerals (i.e. $\Delta\delta^{18}O \approx 30$), corresponding to a ~3% fractional uncertainty in the isotope ratio [74]. The corresponding uncertainty in the antisite defect density is given by,

$$\Delta c \approx \frac{N_O(M_{18} - M_{16})}{N_H(M_D - M_H)}\left(\frac{\Delta\delta^{18}O}{1000} + 1\right)R_0 \tag{8}$$

Assuming the maximum observed uncertainty for $\Delta\delta^{18}$O, the uncertainty in relative density of YAG due to potential variations in isotopic composition is $\sim 2 \times 10^{-6}$, which corresponds to an uncertainty in the antisite defect density of ~0.002 at. %. This is significantly smaller than our experimental uncertainty, showing that natural oxygen isotope variations produce a negligible effect on our results. However, this error is comparable to the uncertainty due to the repeatability specification of the balance, indicating that this would need to be accounted for if a higher precision balance were to be used. Furthermore, this analysis demonstrates that the isotope variations must be considered when analyzing the density of materials that contain multiple isotopes, especially if any minority isotopes have a similar concentration as the majority isotopes.

6. Conclusions

The hydrostatic weighing method was used to measure the density of YAG to probe the intrinsic deviations in stoichiometry present in crystals grown at high temperature by the Czochralski technique. The level of precision afforded by using an absolute density reference along with a refined mechanical design of the measurement apparatus proved to enable reliable calculation of the Y–Al antisites concentration to within ~0.1 atomic percent. It was found that 0.42 ± 0.13 at. % of the C_{3i} symmetry a-sites, typically occupied by Al^{3+}, are instead occupied by Y^{3+} ions. We found the method to be relatively inexpensive, quick, and straightforward to apply and capable of high precision compared to other more widely used material characterization techniques. The hydrostatic weighing method can be implemented for material systems where there are no optical transitions and when the matrix calibration factors required by other methods are unknown. The simplicity of the hydrostatic technique is well suited for evaluating large numbers of samples and potentially providing systematic studies that could be used to optimize the crystal growth process.

Continuing apparatus refinement enables future measurements broadly on other types of defects more broadly, including the density of oxygen vacancies or interstitial oxygen in crystals. For example, we found that the dominant source of error in the measurements arose from the disturbance of the working fluid when placing the sample in the solution. Adopting a simple automated process for placing the samples would significantly increase repeatability, as has been shown in previous work [57,58,61], and we expect that the absolute accuracy of our estimates could be improved by more than a factor of two with that single improvement. Larger samples can decrease error even further, but the increased mass requires a stiffer weighing frame and greater stability to reduce disturbances caused while moving crystals into the fluid. Further improvements to reduce environmental effects can be made by using more elaborate two-body measurement methods [75], or by developing methods employing submerged balances [7,61].

Overall, our approach to hydrostatic weighing is a promising method for efficient, simple, and nondestructive measurements of defect concentrations. With the current precision, the method also works well for quantifying absolute crystal dopant levels of 0.1% or better when there is a significant difference in mass between the dopant and the ion that is replaced in the host lattice.

The method does suffer from the significant requirement to interpret the change in density in terms of specific changes in stoichiometry or unit cell volume, restricting the application to systems where the defect structure is well understood or where specific defect concentrations can be manipulated, such as annealing to change oxygen vacancy densities. As such, this method can provide a novel way to calibrate distribution coefficients for crystal growth of doped materials, for example.

This material is based on work supported by the National Science Foundation under Grant No. OMA-1936350. RK was supported in part by the Montana State University Undergraduate Scholars Program.

Author statement

All authors contributed to all aspects of the work.

Declaration of competing interest

The authors declare that they have no known competing financial interests or personal relationships that could have appeared to influence the work reported in this paper.

Data availability

Data will be made available on request.

Acknowledgments

The authors wish to acknowledge valuable conversations related to this work with S. P. Feofilov regarding his extensive research on defects and disorder in doped garnets, as well as the effects of composition and defects on inhomogeneous broadening and optical decoherence in bulk crystals and nanopowders.

References

[1] R.M. Macfarlane, Y. Sun, R.L. Cone, C.W. Thiel, R.W. Equall, J. Lumin. 107 (2004) 310.
[2] C.W. Thiel, N. Sinclair, W. Tittel, R.L. Cone, Phys. Rev. B 90 (2014), 214301.
[3] C.W. Thiel, N. Sinclair, W. Tittel, R.L. Cone, Phys. Rev. Lett. 113 (2014), 160501.
[4] T. Lutz, L. Veissier, C.W. Thiel, P.J.T. Woodburn, R.L. Cone, P.E. Barclay, W. Tittel, J. Lumin. 191 (2017) 2.
[5] T. Lutz, L. Veissier, C.W. Thiel, P.J.T. Woodburn, R.L. Cone, P.E. Barclay, W. Tittel, Sci. Technol. Adv. Mater. 17 (2016) 63.
[6] O.W. Johnson, J. DeFord, J.W. Shaner, J. Appl. Phys. 44 (1973) 3008.
[7] K. Fujii, Meas. Sci. Technol. 17 (2006) 2551.
[8] G. Wang, Defect and Coherent Transient Optical Spectroscopy of Rare Earth Doped Crystals, Ph.D. thesis, Montana State University, 1997.
[9] G.D. Reinemer, Optical Characterization of Perturbed Sites and C3i Sites in Rare Earth Doped Oxide Crystals, Ph.D. Thesis, Montana State University, 2003.
[10] C.W. Thiel, T. Böttger, R.L. Cone, J. Lumin. 131 (2011) 353.
[11] T. Zhong, P. Goldner, J. Nanophotonics 8 (2019) 2003.
[12] F.A. Selim, D. Solodovnikov, M.H. Weber, K.G. Lynn, Appl. Phys. Lett. 91 (2007), 104105.
[13] V. Laguta, Y. Zorenko, V. Gorbenko, A. Iskaliyeva, Y. Zagorodniy, O. Sidletskiy, P. Bilski, A. Twardak, M. Nikl, J. Phys. Chem. C 120 (2016), 24400.
[14] L. Rogobete, A. Lupei, V. Lupei, A. Petraru, B. Diaconescu, Proc. SPIE 4430 (2001) 97.
[15] S. Ye, F. Xiao, Y.X. Pan, Y.Y. Ma, Q.Y. Zhang, Mater. Sci. Eng. R 71 (2010) 1.
[16] Z.G. Xia, A. Meijerink, Chem. Soc. Rev. 46 (2017) 275.
[17] V. Lupei, A. Lupei, J. Lumin. 169 (2016) 426.
[18] G. Huber, C. Kränkel, K. Petermann, J. Opt. Soc. Am. B 27 (2010) 93.
[19] A.A. Kaminskii, Laser Photon. Rev. 1 (2007) 93.
[20] A. Ikesue, Y.L. Aung, Nat. Photonics 2 (2008) 721.
[21] J.A. Harrington, Proc. SPIE 8959 (2014), 895902.
[22] M. Nikl, A. Yoshikawa, K. Kamada, K. Nejezchleb, C.R. Stanek, Prog. Cryst. Growth Char. Mater. 59 (2013) 47.
[23] Y. Zorenko, A. Voloshinovskii, I. Konstankevych, V. Kolobanov, V. Mikhailin, D. Spassky, Radiat. Meas. 38 (2004) 677.
[24] M.M. Kuklja, R. Pandey, J. Am. Ceram. Soc. 82 (1999) 2881.
[25] M.M. Kuklja, J. Phys. Condens. Matter 12 (2000) 2953.
[26] C. Milanese, V. Buscaglia, F. Maglia, U. Anselmi-Tamburini, Chem. Mater. 16 (2004) 1232.
[27] A.P. Patel, M.R. Levy, R.W. Grimes, R.M. Gaume, R.S. Feigelson, K.J. McClellan, C. R. Stanek, Appl. Phys. Lett. 93 (2008), 191902.
[28] A.B. Muñoz-García, E. Artacho, L. Seijo, Phys. Rev. B 80 (2009), 014105.
[29] B. Liu, M. Gu, X. Liu, S. Huang, C. Ni, Appl. Phys. Lett. 94 (2009), 121910.
[30] Z. Li, B. Liu, J. Wang, L. Sun, J. Wang, Y. Zhou, J. Am. Ceram. Soc. 95 (2012) 3628.
[31] Z. Huang, L. Zhang, W. Pan, J. Eur. Ceram. Soc. 34 (2014) 783.
[32] C. Hu, S. Liu, Y. Shi, H. Kou, J. Li, Y. Pan, X. Feng, Q. Liu, Phys. Status Solidi B 252 (2015) 1993.
[33] S.R. Rotman, C. Warde, J. Appl. Phys. 58 (1985) 522.
[34] M.E. Innocenzi, R.T. Swimm, M. Bass, R.H. French, M.R. Kokta, J. Appl. Phys. 68 (1990) 1200.
[35] X. Xu, Z. Zhao, G. Zhao, P.X. Song, J. Xu, P. Deng, J. Cryst. Growth 257 (2003) 297.
[36] Y. Zorenko, A. Voloshinovskii, V. Savchyn, T. Voznyak, M. Nikl, K. Nejezchleb, V. Mikhailin, V. Kolobanov, D. Spassky, Phys. Status Solidi B 244 (2007) 2180.
[37] C.R. Varney, D.T. Mackay, S.M. Reda, F.A. Selim, J. Phys. D Appl. Phys. 45 (2012), 015103.
[38] N. Shiran, IEEE Trans. Nucl. Sci. 65 (2018) 871.
[39] Y. Sang, D. Yu, M. Avdeev, H. Qin, J. Wang, H. Liu, Y. Lv, J. Solid State Chem. 192 (2012) 366.
[40] M.L. Keith, R. Roy, Am. Mineral. 39 (1954) 1.
[41] S. Geller, Z. Kristallogr. 125 (1967) 1.
[42] S. Geller, G.P. Espinosa, L.D. Fullmer, P.B. Crandall, Mater. Res. Bull. 7 (1972) 1219.
[43] M. Ashurov, Y. Voronko, V.V. Osiko, A.A. Sobol, M.I. Timoshechkin, Phys. Status Solidi A 42 (1977) 101.
[44] J. Dong, K. Lu, Phys. Rev. B 43 (1991) 8808.
[45] R.D. Shannon, Acta Crystallogr. 32 (1976) 751.
[46] A.C. Caballero, F.J. Valle, J.A. Martin Rubi, X Ray Spectrom. 30 (2001) 273.
[47] L. Mariscal-Becerra, M.C. Flores-Jimenez, J.M. Hernandez-Alcantara, E. Camarillo, C. Falcony-Guajardo, R. Vazquez-Arreguin, H.M. Sanchez, J. Nanophotonics 12 (2018), 036013.
[48] P. Lerner, C. Legras, J.P. Dumas, J. Cryst. Growth 3–4 (1968) 231.
[49] K. Nassau, M.E. Lines, J. Appl. Phys. 41 (1970) 533.
[50] L. Kovács, K. Polgár, Cryst. Res. Technol. 21 (1986) K101.
[51] M.N. Palatnikov, I.V. Biryukova, N.V. Sidorov, A.V. Denisov, V.T. Kalinnikov, P.G. R. Smith, V.Ya Shur, J. Cryst. Growth 291 (2006) 390.
[52] U.B. Chanshetti, V.A. Shelke, S.M. Jadhav, S.G. Shankarwar, T.K. Chondhekar, A. G. Shankarwar, V. Sudarsan, M.S. Jogad, Phys. Chem. Technol. 9 (2011) 29.
[53] K. Fujii, M. Tanaka, Y. Nezu, K. Nakayama, H. Fujimoto, P. De Bièvre, S. Valkiers, Metrologia 36 (1999) 455.
[54] P. Hidnert, E.L. Peffer, Natl. Bur. Stand. Circular 487 (1950).
[55] N.A. Pratten, J. Mater. Sci. 16 (1981) 1737.
[56] I. Henins, J. Res. Natl. Bur. Stand. A Phys. Chem. 68A (1964) 529.
[57] H.A. Bowman, R.M. Schoonover, M.W. Jones, J. Res. Natl. Bur. Stand. Sect. C 71 (1967) 179.
[58] K. Fujii, A. Waseda, N. Kuramoto, Meas. Sci. Technol. 12 (2001) 2031.
[59] H. Bettin, H. Toth, Meas. Sci. Technol. 17 (2006) 2567.
[60] P. Becker, H. Friedrich, K. Fujii, W. Giardini, G. Mana, A. Picard, H.-J. Pohl, H. Riemann, S. Valkiers, Meas. Sci. Technol. 20 (2009), 092002.
[61] R.S. Davis, Metrologia 18 (1982) 193.
[62] K. Fujii, Metrologia 41 (2004) S1.
[63] J. Meija, T.B. Coplen, M. Berglund, W.A. Brand, P.D. Bievre, M. Groning, N. E. Holden, J. Irrgeher, R.D. Loss, T. Walczyk, T. Prohaska, Pure Appl. Chem. 88 (2016) 265.
[64] B. Cockayne, D.M. Roslington, A.W. Vere, J. Mater. Sci. 8 (1973) 382.
[65] Omnexus Polymer Properties Database, 2022. https://omnexus.specialchem.com/. (Accessed 28 June 2022). accessed.
[66] R.A. Wach, P. Wolszczak, A. Adamus-Wlodarczyk, Macromol. Mater. Eng. 303 (2018), 1800169.
[67] Z. Li, B. Liu, J. Wang, L. Sun, J. Wang, Y. Zhou, J. Am. Ceram. Soc. 95 (2012) 3628.
[68] R. Wynne, J.L. Daneu, T.Y. Fan, Appl. Opt. 38 (1999) 3282.
[69] V.M. Glazov, A.S. Pashinkin, High Temp. 39 (2001) 413.
[70] Z. Huang, J. Feng, W. Pan, Solid State Sci. 14 (2012) 1327.
[71] W. Martienseen, H. Warlimont (Eds.), Springer Handbook of Condensed Matter and Data Materials, Springer, New York, 2005.
[72] M. Tanaka, G. Girard, R. Davis, A. Peuto, N. Bignell, Metrologia 38 (2001) 301.
[73] L.E. Wright, Oxygen isotopes, in: A.S. Gilbert (Ed.), Encyclopedia of Geoarchaeology, Encyclopedia of Earth Sciences Series, Springer, Dordrecht, 2017, pp. 567–574.
[74] I. Bindeman, Rev. Mineral. Geochem. 69 (2008) 445.
[75] S.I. Toropin, A.B. Lyubomirov, Izmeritel'naya Tekhnika 3 (1988) 28.